



# Chirped polarization volume grating with ultra-wide angular bandwidth and high efficiency for see-through near-eye displays

KUN YIN, HUNG-YUAN LIN, AND SHIN-TSON WU\* 

CREOL, The College of Optics and Photonics, University of Central Florida, Orlando, Florida 32816, USA  
\*swu@creol.ucf.edu

**Abstract:** We report a reflective chirped polarization volume grating (CPVG) with a dramatically wider angular bandwidth and significantly higher first-order diffraction efficiency than the holographic volume grating and surface relief grating for large field-of-view (FOV) augmented reality (AR) displays. By introducing gradient pitch structure along the beam propagation direction, the angular bandwidth is extended from  $18^\circ$  to  $54^\circ$  while keeping over 80% diffraction efficiency. We also prepare a two-layer reflective PVG and compare its performance with the chirped structure. Based on the simulation and experimental results, CPVG is a strong contender for large FOV AR displays.

© 2019 Optical Society of America under the terms of the [OSA Open Access Publishing Agreement](#)

## 1. Introduction

Augmented reality (AR) displays, such as Google Glass, Microsoft HoloLens and Magic Leap One, have found widespread applications. To maintain the see-through capability, an optical combiner to overlay the computer-generated images with environment is often employed. Different types of optical combiners, such as polarizing beam splitter, partial mirror, grating-based waveguide, have been demonstrated. Among them, waveguide-based combiner offers several attractive features, such as compact structure, lightweight, and wide field-of-view (FOV). In the waveguide structure, holographic volume grating (HVG) [1,2] and surface relief grating (SRG) [3] are commonly used as the input/output combiners. Similar to Volume Bragg Grating (VBG), HVG possesses a large diffraction angle and high efficiency. The angular bandwidth of HVG is determined by the index contrast. Based on dichromated gelatin (a common material for HVG), the index contrast can reach as high as 0.15 [4]; however, the dichromated gelatin is environmentally sensitive and therefore it is not suitable for commercial products. Thus, a more commonly used material for making HVG is a photo-polymer having refractive index contrast of about 0.035 [5], which results in a limited FOV (angular bandwidth  $\leq 10^\circ$ ) [6,7]. In terms of SRG, due to the large index contrast between polymer and air, SRG can achieve a larger angular bandwidth ( $\sim 25^\circ$ ) than HVG [8,9]; and this tilted-groove structure is achieved by nanoimprinting method in mass production. When fabricating large tilt angle structures, the yield of this method has yet to be improved [3]. Similar to HVG, SRG also has to address the tradeoff between angular bandwidth, diffraction efficiency, and manufacturing cost. As a result, the FOV of the latest released waveguide-based AR products, such as Microsoft HoloLens 2 and Magic Leap One, is still limited by the combiner and total internal reflection (TIR). Therefore, there is an urgent need to increase the FOV of AR displays.

Recently, extensive efforts have been attempted to applying reflective polarization volume grating (PVG) for waveguide coupling [10–13]. Compared to HVG and SRG, reflective PVG based on liquid crystal materials exhibits unique characteristics in both optical properties and fabrication, such as nearly 100% first-order diffraction efficiency, high index contrast, large diffraction angle, strong polarization selectivity, and simple fabrication process. The pioneering work on reflective PVGs has experimentally achieved 95% diffraction efficiency; in addition, a

stretchable and flexible PVG film is also investigated [14]. However, the angular bandwidth is still inadequate for AR waveguide applications [15].

In this paper, we demonstrate a reflective chirped polarization volume grating (CPVG) for widening the FOV of see-through near-eye displays. The CPVGs, with the grating period gradually changing along the beam propagation, not only inherit the advantages of PVGs but also triple the angular bandwidth. We fabricated such a wide-angular-bandwidth CPVG and characterized its performance. The measured results are consistent with the simulation ones using the finite-element method (FEM). Besides, we also investigate the performance of multi-layer PVGs by simulation. In experiment, we fabricated a two-layer PVG and compared its performance with CPVGs. To the best of our knowledge, both CPVGs and multi-layer reflective PVGs have not been reported before.

## 2. Device design and simulation

In a conventional cholesteric liquid crystal (CLC), the helical twist in the vertical direction is induced by the doped chiral compound, while the LC directors are uniform in the horizontal plane. By contrast, a PVG exhibits uniform molecular rotation with respect to a slanted helical axis, as Fig. 1(a) illustrates. The horizontal periodicity ( $\Lambda_x$ ) is defined as the distance by which LC directors rotate  $180^\circ$  along the horizontal direction, and the vertical periodicity ( $\Lambda_y$ ) is the distance by which LC directors rotate  $180^\circ$  along the vertical direction. The relationship between Bragg periodicity ( $\Lambda_B$ ),  $\Lambda_x$  and  $\Lambda_y$  can be described as:

$$\frac{1}{\Lambda_x^2} + \frac{1}{\Lambda_y^2} = \frac{1}{\Lambda_B^2}. \quad (1)$$

In order to obtain a wider angular bandwidth, we induce gradually changing period along  $y$  direction as a modulation while the period along  $x$  direction is fixed. Several approaches to generate gradient pitch in CLC have been reported in [16,17]. By adding UV dye into the PVG precursor, raising the curing temperature, and decreasing the power of UV curing light, we can precisely control the length of  $\Lambda_B$ , which is determined by the CLC structure. As reported in [18], the  $\Lambda_B$  along the helical axis is defined by:

$$\frac{1}{\Lambda_B} = \frac{1}{\Lambda_{B1}} + \left( \frac{1}{\Lambda_{B2}} - \frac{1}{\Lambda_{B1}} \right) \frac{s}{t}, \quad (2)$$

where  $t$  is the total length of the helical axis and  $s$  is the coordinate along it, and the period lengths are gradually changing from  $\Lambda_{B1}$  ( $s=0$ ) to  $\Lambda_{B2}$  ( $s=t$ ). By applying Eqs. (1) and (2) to the CPVG model while keeping  $\Lambda_x$  as a constant, we derive the variation of  $\Lambda_y$  along  $y$  direction in CPVG as:

$$\frac{1}{\Lambda_y} = \frac{1}{\Lambda_{y1}} + \left( \frac{1}{\Lambda_{y2}} - \frac{1}{\Lambda_{y1}} \right) \frac{y}{d} + o \left( \frac{(\Lambda_{y1} - \Lambda_{y2})^2}{\Lambda_{y1}^3} \right), \quad (3)$$

where  $\Lambda_{y1}$  and  $\Lambda_{y2}$  are the period lengths along  $y$  axis near the bottom surface and top surface, respectively, and  $o$  means the higher-order terms. Generally,  $(\Lambda_{y1} - \Lambda_{y2})^2 / \Lambda_{y1}^3$  is much smaller than 1 so that this term can be omitted safely, similar to that reported in [19]. Furthermore, the equation of the isophase line in CPVG can be expressed as:

$$\Phi_{gradient,CPVG} = \frac{\pi}{\Lambda_x} x + \frac{\pi}{\Lambda_{y1}} y + \left( \frac{\pi}{\Lambda_{y2}} - \frac{\pi}{\Lambda_{y1}} \right) \frac{y^2}{d}, \quad (4)$$

where  $\Lambda_x$  is the period length along  $x$  axis and  $d$  is the thickness of CPVG. As shown in Fig. 1(b), the length of  $\Lambda_B$  gradually increases from  $\Lambda_{B1}$  to  $\Lambda_{B2}$ , and the length of corresponding  $\Lambda_y$  also increases from  $\Lambda_{y1}$  to  $\Lambda_{y2}$ . Once the isophase line equation is derived, we can obtain the LC

orientations inside the CPVG. These orientations define the dielectric constant matrix, which is the key parameter in the simulation. Compared to a uniform PVG, the gradient pitch profile generates a series of refractive index planes with gradually changing slope.

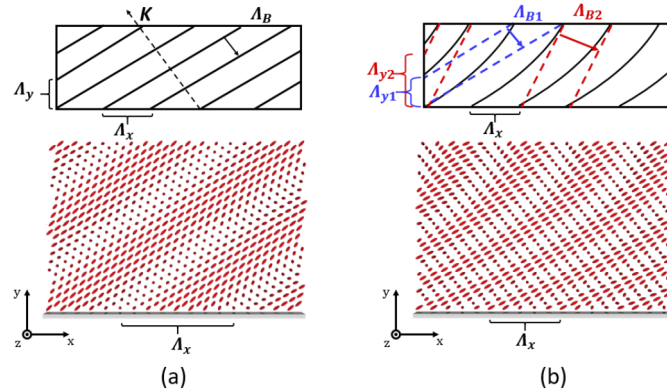


**Fig. 1.** LC director profile of the uniform PVGs and CPVGs. (a) the horizontal period is  $\Lambda_x$ , the vertical period is  $\Lambda_y$ , and the Bragg period is  $\Lambda_B$ . (b) The horizontal periodicity is  $\Lambda_x$ , the vertical periodicities are  $\Lambda_{y1}$  and  $\Lambda_{y2}$  at the bottom and top, respectively, and the Bragg period are  $\Lambda_{B1}$  and  $\Lambda_{B2}$  at the bottom and top, respectively.

In simulation, we assume the birefringence of a reactive mesogen RM257 is  $\Delta n = 0.18$  ( $n_e = 1.68$ ,  $n_o = 1.50$ ) at  $\lambda = 532$  nm and the thickness of the grating is  $5 \mu\text{m}$ . For a uniform PVG, the period length along  $x$  and  $y$  directions are set as  $\Lambda_x = 462$  nm and  $\Lambda_y = 203$  nm. In terms of CPVGs, the length of  $\Lambda_{y1}$  and  $\Lambda_{y2}$  are set as 192 nm and 203 nm, respectively. The simulated angular response for the gradient pitch (CPVGs) and uniform pitch (PVGs) are depicted in Fig. 2. The black curve in Fig. 2(a) shows the angular bandwidth of such a uniform PVG is around  $18^\circ$  ( $-8^\circ$  to  $10^\circ$ ) at 80% efficiency (marked with gray dashed lines). In comparison with uniform PVGs, CPVGs have the angular bandwidth of  $57^\circ$  (from  $-9^\circ$  to  $48^\circ$ ) with diffraction efficiency over 80%. Our results clearly demonstrate that inducing gradient pitch significantly broadens the angular bandwidth. We also simulate the angular and spectral bandwidth of CPVGs and results are shown in Fig. 2(b).

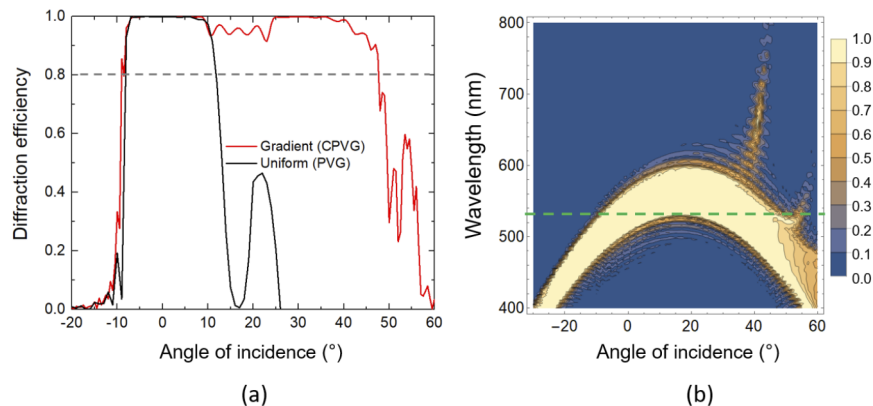


**Fig. 2.** Simulated first-order diffraction efficiency: (a) angular response at  $\lambda = 532$  nm of both gradient pitch CPVGs (red line) and uniform pitch PVG (black line); and (b) simulated angular and spectral responses of the CPVGs. The green dashed lines indicate  $\lambda = 532$  nm.

### 3. Experiment

#### 3.1. Fabrication of CPVG

The fabrication procedure of reflective CPVGs is similar to that described in [14] except for different precursor and UV curing condition. We firstly spin-coated brilliant yellow (dissolved in dimethylformamide with 0.40 wt%) onto a cleaned glass substrate as photo-alignment layer, and then put the sample in a Mach-Zehnder interferometer ( $\lambda = 488 \text{ nm}$ ) to get exposure. The two-beams that interfere at the sample are left-handed circularly polarized (LCP) and right-handed circularly polarized (RCP), respectively. Next, we spin-coated the PVG precursor onto the exposed sample. The mixture consisting of 1.50 wt% UV dye (Avobenzene), 2.48 wt% chiral agent R5011 (HCCH, helical twisting power HTP  $\approx 108 \text{ /}\mu\text{m}$ ), 3.00 wt% initiator Irgacure 651, and 93.02 wt% photocurable monomer RM257 (HCCH) was diluted in toluene. To generate gradient pitch, the sample was placed on a hot plate at  $60^\circ\text{C}$  and cured with UV light ( $\lambda = 365 \text{ nm}$ ,  $0.3 \text{ mW/cm}^2$ ) for 40 minutes in nitrogen environment. Then a CPVG working on green (532 nm) light was obtained. By controlling the concentration of the chiral agent, we can easily get different central wavelengths in the visible range, such as red (633 nm) and blue (473 nm).

#### 3.2. Two-layer PVGs

To fabricate a two-layer PVG, two different precursors are used. The first mixture consisting of 2.31 wt% chiral agent R5011, 3.00 wt% photo-initiator Irgacure 651, and 94.69 wt% photocurable monomer RM257 was diluted in toluene. The second mixture consisting of 2.62 wt% R5011, 3.00 wt% Irgacure 651, and 94.38 wt% RM257. To generate two-layer structure, the first mixture was spin-coated and then cured with UV light ( $\lambda = 365 \text{ nm}$ ,  $12 \text{ mW/cm}^2$ ) for 5 minutes in nitrogen environment. Next, the second mixture was spin-coated onto the first layer and cured at the same conditions. The multi-layer PVGs can also be fabricated following this strategy. We measured the optical properties with a glass cylinder container filled with index matching oil ( $n = 1.58$ ), as described in [13]. The CPVG sample was mounted on a rotatable stage and the whole unit was immersed in the container. The incident light was normal to the CPVG at the initial state, and the angle of incidence can be adjusted by rotating the CPVG. The first-order diffracted beam was measured by a power meter. The efficiency is defined as the intensity of the diffracted beam to that of the reference beam passing through the glass cylinder with index matching oil and glass substrate only (without CPVGs).

#### 3.3. Results

We first measured the angular response of CPVG using a circularly polarized green ( $\lambda = 532 \text{ nm}$ ) laser diode, and results are shown in Fig. 3(a). The angular bandwidth is  $54^\circ$  (from  $-7^\circ$  to  $47^\circ$ ) at 80% diffraction efficiency. Compared to a uniform PVG, the angular bandwidth is 3x wider. The inset photo is viewed at  $50^\circ$  to clearly see the diffracted green light from the CPVG sample, where the CPVG region is circled by the blue line. The text shown in Fig. 3(b) was imaged through the sample. The distance between CPVG and camera is 1 cm, and the target is 10 cm away. The clear image seen through the CPVG region (encircled by the blue line) indicates that the scattering of the grating film is negligible. Due to the handedness selectivity, this CPVG allows more than 50% transmittance of the ambient light when the circularly polarized input is out-coupled at 80% efficiency. By introducing chirped structure to conventional PVGs, we can obtain a wide angular bandwidth, while keeping high efficiency and low scattering for a large-FOV AR display. The angular bandwidth of CPVG is  $\sim 2\text{x}$  larger than that of SRG, and  $\sim 3\text{x}$  larger than that of PVG and HVG. From Fig. 3(a), the experimental data are in a reasonably good agreement with the simulation results, although the measured diffraction efficiency is about 10% lower than the simulated one. The main reason is that the LC alignment is quite sophisticated,

including horizontal subwavelength period and vertical gradient period. Any disturbed alignment would decrease the diffraction efficiency.

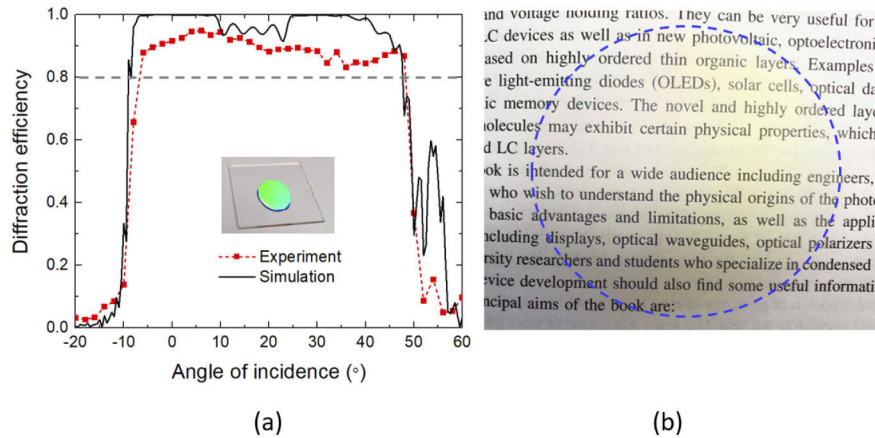


**Fig. 3.** (a) Angular behavior of optical efficiency. The red dots denote the measured results of CPVG sample. Inset: a CPVG sample viewed from an oblique angle with the CPVG region circled by the blue line. (b) A photo taken through the CPVG sample. CPVG region is circled in the blue line. The distance between PVG to camera was 1 cm, and the target was 10 cm away.

**4. Discussion**

The CPVGs exhibit excellent optical properties and simple fabrication process. Similar to gradually changing period, discretely changed period can also extend the angular bandwidth. Figure 4(a) illustrates the concept of multi-layer structure. When the number of layers  $N$  approaches positive infinity, the multi-layer PVGs behave like CPVGs. Therefore, we would like to compare the performance of multi-layer PVGs with CPVGs.

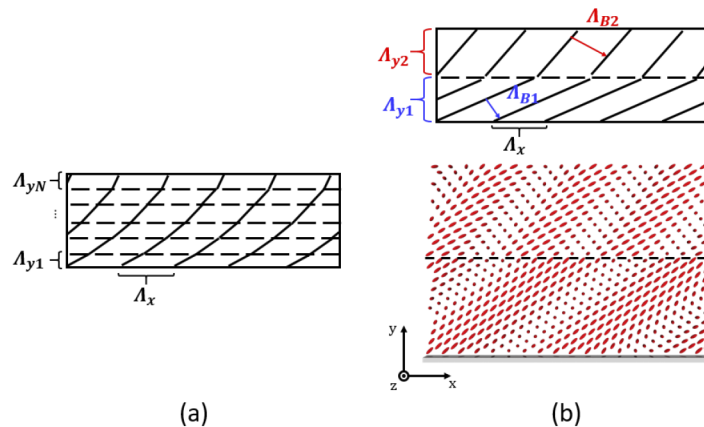


**Fig. 4.** (a) LC director profile of a multi-layer PVG. The horizontal period is  $\Lambda_x$ , the number of layers is  $N$ , the vertical period is  $\Lambda_{y1}$  to  $\Lambda_{yN}$ , respectively. (b) The horizontal periodicity is  $\Lambda_x$ , the vertical periodicity is  $\Lambda_{y1}$  for the bottom layer and  $\Lambda_{y2}$  for the top layer. The gray dashed lines show the top surface of the bottom layer.

For the  $i$ -th layer ( $i$  from 1 to  $N$ ), the twist angle in the isophase plane of multi-layer PVGs is defined by:

$$\Phi_{i,\text{multi-layer,PVG}} = \frac{\pi}{\Lambda_x}x + \frac{\pi}{\Lambda_{y_i}}\frac{y}{d_i} + \Phi_i, \quad (5)$$

where  $\Lambda_x$  is the surface period,  $\Lambda_{y_i}$  is the period of  $i$ -th layer,  $d_i$  is the thickness of the  $i$ -th layer. To simplify the simulation and fabrication processes, we set  $N=2$  and take this two-layer structure as an example to reveal the features of multi-layer structure. As shown in Fig. 4(b), the length of horizontal period is  $\Lambda_x$  and the length of vertical period for each layer is  $\Lambda_{y1}$  and  $\Lambda_{y2}$ , respectively. Although the vertical periods are different, each layer is uniform and follows the variation of uniform PVGs.

In simulation, we assume  $\Delta n = 0.18$  at  $\lambda = 532$  nm. To keep consistency, the parameters of uniform PVGs are still set as  $\Lambda_x = 462$  nm and  $\Lambda_y = 203$  nm. For the two-layer PVG, the period length is assumed to be  $\Lambda_x = 462$  nm along  $x$ -axis, and  $\Lambda_{y1} = 190$  nm and  $\Lambda_{y2} = 220$  nm along  $y$ -axis and the thickness of each layer is  $2.5$   $\mu\text{m}$ . The simulated and measured angular responses for the two-layer PVG are depicted in Fig. 5(a). The angular bandwidth of the two-layer PVG can also be extended to  $60^\circ$ , but the average efficiency is lower than  $80\%$ . The measured results generally agree with the simulated ones, except for lower optical efficiency. Due to the two-layer structure, the alignment of the second layer is highly dependent on the alignment of the first layer. Any defect in the first layer will affect the following layers, which in turn leads to the decreased optical efficiency. The angular bandwidth of the two-layer PVGs is experimentally extended to  $65^\circ$  (from  $-10^\circ$  to  $55^\circ$ ) with  $20\%$  diffraction efficiency and an average efficiency of more than  $60\%$ . It is worth noting that there are two deep valleys (at  $0^\circ$  and  $40^\circ$ ) in the angular response band. The diffraction efficiency at the valleys drops significantly, so this two-layer PVG is not suitable for AR displays that require a uniform image with high efficiency.

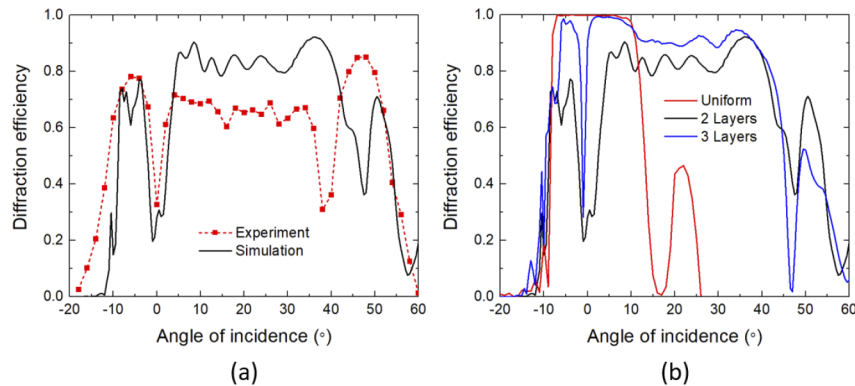


**Fig. 5.** (a) Simulated and measured angular behavior of two-layer PVG. The red dots denote the experimental results; (b) Simulated first-order diffraction efficiency and angular response at  $\lambda = 532$  nm of uniform PVG (red line), two-layer PVG (black line), and three-layer PVG (blue line).

Here we only fabricate a two-layer ( $N=2$ ) structure to illustrate the calculation methods and fabrication process of a multi-layer structure. As the number of layers increases, the multi-layer PVGs will behave like CPVGs. When  $N=3$ , the period length is assumed to be  $\Lambda_x = 462$  nm along  $x$ -axis,  $\Lambda_{y1} = 190$  nm,  $\Lambda_{y2} = 205$  nm, and  $\Lambda_{y3} = 220$  nm along  $y$ -axis. The thickness of each layer is  $1.67$   $\mu\text{m}$ . All the simulation results ( $N=1, 2, 3$ ) are shown in Fig. 5(b). Compared to the two-layer PVG, the three-layer PVG has a better angular performance (from  $-10^\circ$  to  $15^\circ$ ) and a higher average diffraction efficiency. Furthermore, by inducing more variables, such as the number of layers ( $i$ ), the thickness ( $d_i$ ), and the vertical period ( $\Lambda_{y_i}$ ) into the multi-layer

structure, both the angle response and efficiency can be optimized. To obtain an optimal solution, a multi-layer structure can be simulated using rigorous-coupled-wave-analysis (RCWA) [20]. It is possible to get both wide angular bandwidth and high efficiency as well as CPVGs.

In comparison with CPVGs, the biggest challenge for achieving wide angular bandwidth in multi-layer PVGs is not the optimization method but the fabrication process. Due to the roughness on the top surface of polymerized LC film, it is not easy to precisely control the thickness and the twist angle of each layer. The more layers we need, the more defects will be induced into the volume gratings. In addition, the LC molecules follow the pattern of the previous layer, therefore any kind of defects including unaligned molecules or dust will have a serious effect on all the following layers.

## 5. Conclusion

We have experimentally demonstrated CPVGs with an extra-large angular bandwidth while keeping optical efficiency over 80%. This is achieved by inducing gradient pitch along the beam propagation direction. Specifically, our CPVG possesses 54° angular bandwidth, over 80% average efficiency, and 95% peak efficiency. These results represent the widest angular bandwidth and highest diffraction efficiency ever demonstrated for diffraction gratings in a comparable configuration, including HVGs and SRGs. Besides, we also explore the multi-layer PVG structure and take a two-layer PVG as an example to illustrate the simulation method and fabrication process. Compared to a multi-layer PVG, CPVG exhibits better optical performance and simpler fabrication process. Due to the wide angular bandwidth, high efficiency, low scattering, high transmittance, and simple fabrication, CPVG would be a strong contender for see-through near-eye displays.

## Funding

GoerTek Electronics.

## Disclosures

The authors declare no conflicts of interest.

## References

1. I. Kasai, Y. Tanijiri, E. Takeshi, and U. Hiroaki, "A practical see-through head mounted display using a holographic optical element," *Opt. Rev.* **8**(4), 241–244 (2001).
2. H. Mukawa, K. Akutsu, I. Matsumura, S. Nakano, T. Yoshida, M. Kuwahara, and K. Aiki, "A full-color eyewear display using planar waveguides with reflection volume holograms," *J. Soc. Inf. Disp.* **17**(3), 185–193 (2009).
3. B. C. Kress and W. J. Cummings, "Towards the ultimate mixed reality experience: HoloLens display architecture choices," *Dig. Tech. Pap. - Soc. Inf. Disp. Int. Symp.* **48**(1), 127–131 (2017).
4. T. Rasmussen, "Overview of high-efficiency transmission gratings for molecular spectroscopy," *Spectroscopy (Springf.)* **29**(4), 32–39 (2014).
5. F. Bruder, T. Fäcke, R. Hagen, D. Hönel, E. Orselli, C. Rewitz, T. Rölle, and G. Walze, "Diffractive optics with high Bragg selectivity: volume holographic optical elements in Bayfol® HX photopolymer film," *Proc. SPIE* **9626**, 96260T (2015).
6. N. Zhang, J. Liu, J. Han, X. Li, F. Yang, X. Wang, B. Hu, and Y. Wang, "Improved holographic waveguide display system," *Appl. Opt.* **54**(12), 3645–3649 (2015).
7. M. J. Escuti, P. Kossyrev, G. P. Crawford, T. G. Fiske, J. Colegrove, and L. D. Silverstein, "Expanded viewing-angle reflection from diffuse holographic-polymer dispersed liquid crystal films," *Appl. Phys. Lett.* **77**(26), 4262–4264 (2000).
8. T. M. de Jong, D. K. de Boer, and C. W. Bastiaansen, "Surface-relief and polarization gratings for solar concentrators," *Opt. Express* **19**(16), 15127–15142 (2011).
9. B. Bai, J. Laukkanen, M. Kuittinen, and S. Siitonen, "Optimization of nonbinary slanted surface-relief gratings as high-efficiency broadband couplers for light guides," *Appl. Opt.* **49**(28), 5454–5464 (2010).
10. J. Kobashi, H. Yoshida, and M. Ozaki, "Planar optics with patterned chiral liquid crystals," *Nat. Photonics* **10**(6), 389–392 (2016).

11. J. Kobashi, Y. Mohri, H. Yoshida, and M. Ozaki, "Circularly-polarized, large-angle reflective deflectors based on periodically patterned cholesteric liquid crystals," *Opt. Data Process. Storage* **3**(1), 61–66 (2017).
12. Y. H. Lee, K. Yin, and S. T. Wu, "Reflective polarization volume gratings for high efficiency waveguide coupling augmented reality displays," *Opt. Express* **25**(22), 27008–27014 (2017).
13. Y. H. Lee, Z. He, and S. T. Wu, "Optical properties of reflective liquid crystal polarization volume gratings," *J. Opt. Soc. Am. B* **36**(5), D9–D12 (2019).
14. K. Yin, Y. H. Lee, Z. He, and S. T. Wu, "Stretchable, flexible, rollable, and adherable polarization volume grating film," *Opt. Express* **27**(4), 5814–5823 (2019).
15. Y. H. Lee, G. Tan, K. Yin, T. Zhan, and S. T. Wu, "Compact see-through near-eye display with depth adaption," *J. Soc. Inf. Disp.* **26**(2), 64–70 (2018).
16. D. J. Broer, J. Lub, and G. N. Mol, "Wide-band reflective polarizers from cholesteric polymer networks with a pitch gradient," *Nature* **378**(6556), 467–469 (1995).
17. D. Katsis, D. U. Kim, H. P. Chen, L. J. Rothberg, S. H. Chen, and T. Tsutsui, "Circularly polarized photoluminescence from gradient-pitch chiral-nematic films," *Chem. Mater.* **13**(2), 643–647 (2001).
18. Q. Hong, T. X. Wu, and S. T. Wu, "Optical wave propagation in a cholesteric liquid crystal using the finite element method," *Liq. Cryst.* **30**(3), 367–375 (2003).
19. Y. Weng, D. Xu, Y. Zhang, X. Li, and S. T. Wu, "Polarization volume grating with high efficiency and large diffraction angle," *Opt. Express* **24**(16), 17746–17759 (2016).
20. X. Xiang, J. Kim, and M. J. Escuti, "Bragg polarization gratings for wide angular bandwidth and high efficiency at steep deflection angles," *Sci. Rep.* **8**(1), 7202 (2018).